Chapter 6
Ion impact ionization of atoms and molecules : Comparative study at keV and MeV energy

6.1 Introduction

In this chapter we will discuss about the DDCS of electron emission from atomic and molecular targets induced by keV and MeV energy ions. The ionization studies were performed on three different targets, such as, He, CH_4 and O_2 in collisions with keV energy protons. In case of O_2, measurements were also performed with MeV energy C^{6+} ions. The goal of the present series of measurements was to understand how the ionization dynamics change with the variation in the velocity (v_p) and charge state (q_p) of the projectiles. In case of He, DDCS measurements were carried out using 150 and 200 keV protons. For methane, collisions were performed using 200 keV protons and for O_2, the projectiles were 200 keV protons and 66 MeV C^{6+} ions. All these projectiles were chosen such that, the charge state (q_p) and velocity (v_p) are widely different, but their perturbation strength (q_p/v_p) are nearly the same i.e., 0.35 for the 200 keV/u protons, 0.41 for 150 keV/u protons and 0.40 for the 5.5 MeV/u C^{6+} ions. In the past decades, several experimental and theoretical studies have been performed for the DDCS of electron emission from helium in collisions with protons and highly charged ions having energies from few keV to several MeV [139, 140, 141, 142, 143, 144, 145, 146, 147, 148, 149, 150, 151, 152, 153, 154, 155]. On the other hand, not many DDCS measurements have been reported in case of CH_4 and O_2 [156, 157, 158, 159, 160, 161, 162], although these molecules have been explored from other channels like ionization, fragmentation, charge transfer processes [163, 164, 165, 166].

In addition to understanding the variation in the collision dynamics due to change in q_p and v_p, these e-DDCS measurements provide a stringent test for checking the efficacy of the different theoretical models which are used for studying ion-atom collisions. For 5.5 MeV/u C^{6+} ions, the velocity of the projectile being quite high, i.e., $v_p \sim 15$ a.u., most of the perturbative models are expected to work well in this regime. However, for 150 and 200 keV protons, the projectile velocities are $\sim$ 2.4 and 2.8 a.u., respectively, i.e., closer to the intermediate velocity regime and hence along with the ionization, electron capture and transfer ionization channels are also effective. In most of the earlier work on DDCS measurements of electron emission from He by proton impact that are cited above, the measured data were compared with the first Born approximation which is a one center model and is well known to work only for projectiles with high energy. It does not take into account the post collisional effects. On the other hand,

the CDW-EIS model assumes the ionized electron to be influenced by the long-range Coulomb field of both the target and the projectile centers and hence explains the two-centre effect accurately. Thus the CDW-EIS model is effective for both the intermediate and high energy regime of the projectile. It is noteworthy to mention that the present series of experiments using both He-atom and simple molecules along with the elaborate comparison with the CDW-EIS model provide a new set of inputs for understanding the collision dynamics at both the intermediate and high velocity regime of the projectiles. Further, these small molecular targets like O_2 and CH_4 serve as a bridge between the small atoms and large molecules (e.g. biomolecules) and thus provide an accurate testing of the theoretical models before they are applied for the larger molecules which will be seen in the next chapter.

6.2 Experimental details

The first part of the present measurements were carried out for collisions of protons with He, CH_4 and O_2 molecules. The keV energy protons were generated from the ECR Ion Accelerator. The details of the experimental set up is described in chapter 2 and in our recent publication [167]. In brief, an extraction voltage of 30 kV was applied at the ion source whereas the deck voltage was raised to 120 kV for producing 150 keV protons and 170 kV for 200 keV protons. The experiments were performed both under static gas pressure condition as well as an effusive jet source was used for some cases. For static pressure condition, the chamber was filled with He gas at an absolute pressure of 0.1 mTorr and for CH_4 it was set to 0.05 mTorr. The cross section being quite high for the chosen velocity regime, the statistical error was low and it varied from $\sim$ 1% to 4%.

The second part of the experiment was carried out with the 66 MeV C^{6+} ions in collisions with O_2 molecules. The MeV energy bare C ions were produced from the TIFR-BARC Pelletron accelerator. Initially, C^{5+} ions of desired energy were selected and then passed through a post-stripper carbon foil arrangement to obtain the bare ions. The bare C ions were then selected by a switching magnet and directed to the desired beamline. The scattering chamber was filled with the O_2 gas at an absolute pressure of 0.15 mTorr. The hemispherical electrostatic energy analyzer along with CEM were used to measure the ionized electrons. The maximum statistical error for these measurements was $\sim$ 8% to 9%.

6.3 Double differential cross sections

Figure 6.1 and Figure 6.2 display the absolute DDCS of the electrons emitted due to single ionization of He in collisions with 150 keV and 200 keV protons, respectively. In either cases, the DDCS have been shown for eight different electron emission angles. It is seen that the DDCS falls by several orders of magnitude with the increase in emission energy for a given

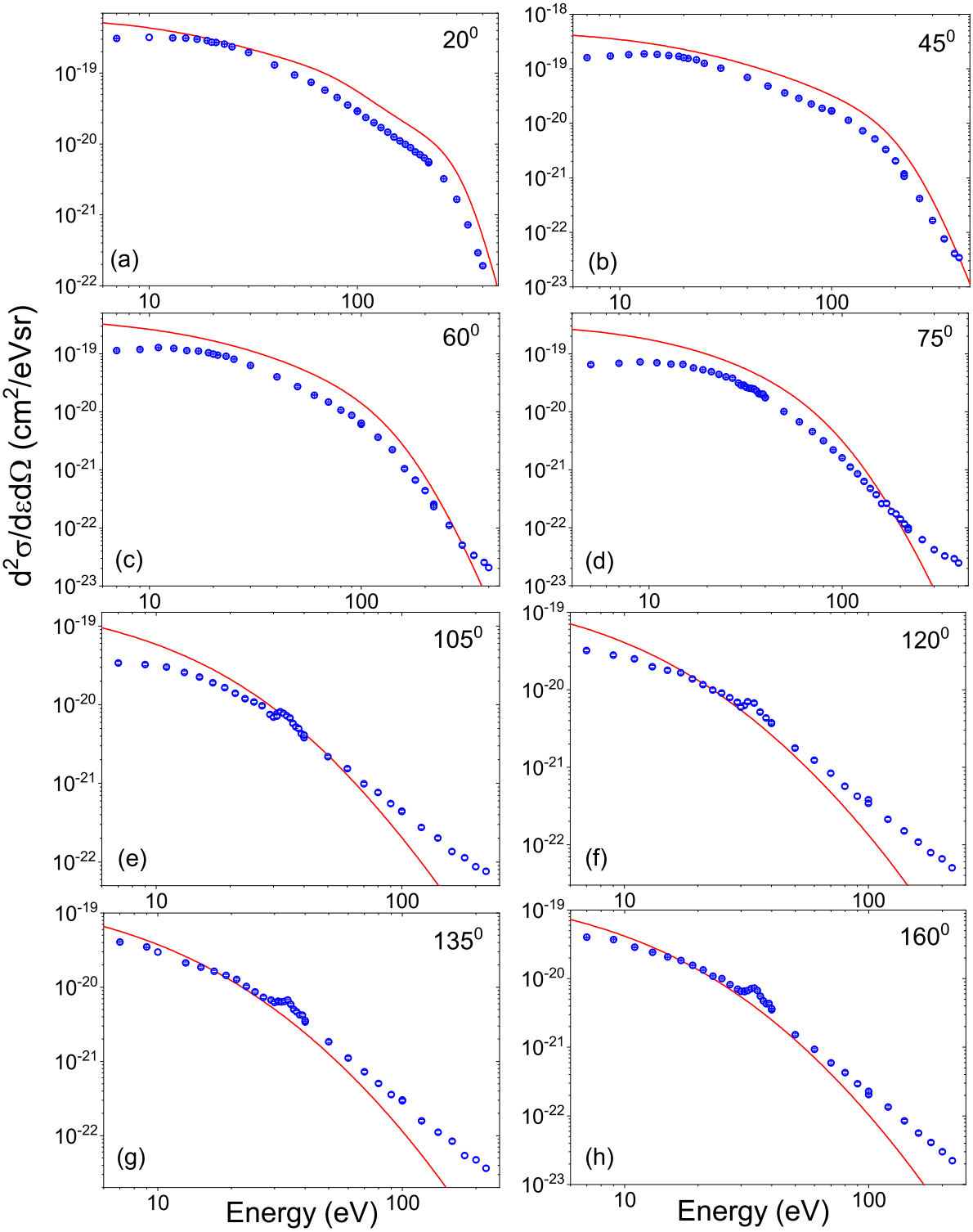

Figure 6.1: Absolute electron DDCS for the collision system 150 keV proton + He shown at eight different emission angles. The CDW-EIS calculations are represented by the red solid lines.

emission angle. A small peak is seen in case of the backward angles at around 35 eV which corresponds to the autoionization process. In this process, two electrons are excited simultaneously, and then subsequently one electron goes to the ground state, giving off the excess energy

to the other electron which is then emitted with the specified energy. The Coulomb ionization contribution being large for the forward angles, the characteristic autoionization peak is not observed.

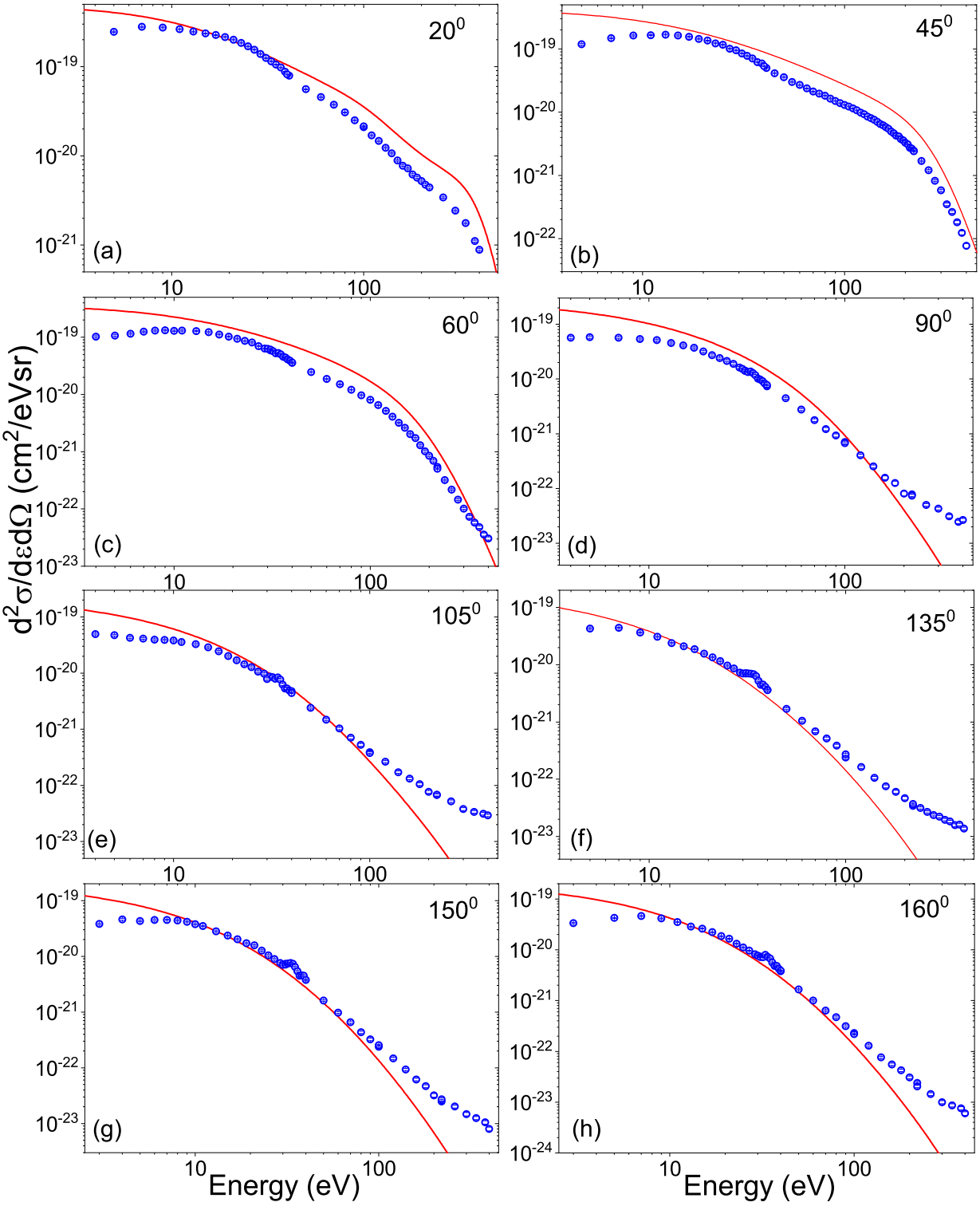

Figure 6.2: Absolute electron DDCS for the collision system 200 keV proton + He along with the CDW-EIS calculations shown by the red solid lines.

The red solid line in either figures show the calculations obtained using the prior form of

the Continuum Distorted Wave-Eikonal Initial State (CDW-EIS) model. In this model the independent particle approximation is employed which considers only one electron of each one of the atomic orbitals to be ionized whereas all the other target electrons i.e., the passive electrons are considered to remain as frozen in their initial orbitals. In this formalism, the straight line version of the impact parameter approximation [64, 168] is used for the calculations . In the prior form of the CDW-EIS approximation, the scattering amplitude is expressed as a function of the impact parameter in the following manner [169]:

$$\mathcal{A}_{if}^{-}(\rho) = -i \int_{-\infty}^{+\infty} dt \left\langle \chi_f^{-} \middle| \left[\left(H_{el} - i \frac{\partial}{\partial t} \right) \middle| \chi_i^{+} \right\rangle \right] \tag{6.1}$$

where H_{el} is the one-active-electron Hamiltonian whereas χ_i^+ and χ_f^- are the initial and final channel distorted wave functions respectively, given by

$$\chi_i^+ = \varphi_i(\mathbf{x}) \, \exp\left(-i\,\varepsilon_i\,t\right) \, \exp\left[-i\,\nu \, \ln\left(v\,s + \mathbf{v}\cdot\mathbf{s}\right)\right] \tag{6.2}$$

$$\begin{aligned} \chi_f^- =& \varphi_f(\mathbf{x}) \, \exp\left(-i\,\varepsilon_f\,t\right) \\ & \times \; N^*(\lambda) \, {}_1F_1[-i\,\lambda; 1; -i(k\,x - \mathbf{k}\cdot\mathbf{x})] \\ & \times \; N^*(\xi) \, {}_1F_1[-i\,\xi; 1; -i(p\,s - \mathbf{p}\cdot\mathbf{s})] \end{aligned} \tag{6.3}$$

being $\mathbf{x}$ ($\mathbf{s}$) the active-electron coordinate in a target-fixed (projectile-fixed) reference frame. In (Equation 6.2) φ_i corresponds to the active electron initial bound state and ε_i is its initial binding energy, $\nu = Z_P/v$ with Z_P being the projectile charge and v is the collision velocity. In (Equation 6.3) φ_f is a free-electron plane wave with momentum $\mathbf{k}$, $\varepsilon_f = \frac{1}{2}\,k^2$, $\xi = Z_P/p$, being $\mathbf{p} = \mathbf{k} - \mathbf{v}$, $\lambda = \tilde{Z}_T/k$ with $\tilde{Z}_T$ and effective target nuclear charge describing the interaction of the active electron with an effective residual target Coulomb potential. ${}_1F_1$ is the hypergeometric function and $N(a) = \exp\left(\pi\,a/2\right)\Gamma(1 - i\,a)$ is its normalization factor (with Γ the Euler Gamma function).

For the He target, the initial bound state of the atom was considered within a Roothaan-Hartree-Fock (RHF) representation [102]. The residual target continuum state effective charge is considered as

$$\tilde{Z}_T = n_i \sqrt{-2\,\varepsilon_i} \tag{6.4}$$

In case of Helium, n_i is the principal quantum number of the atomic orbital and ε_i its ionization energy.

The CDW-EIS model shows qualitatively an overall good agreement with the data for all the forward angles although quantitatively overestimates the measured data points (see Figure 6.1 and Figure 6.2). For the backward angles, the model is seen to match well with the data points upto about 50 to 70 eV, beyond which it underestimates the data for the rest of the spectra.

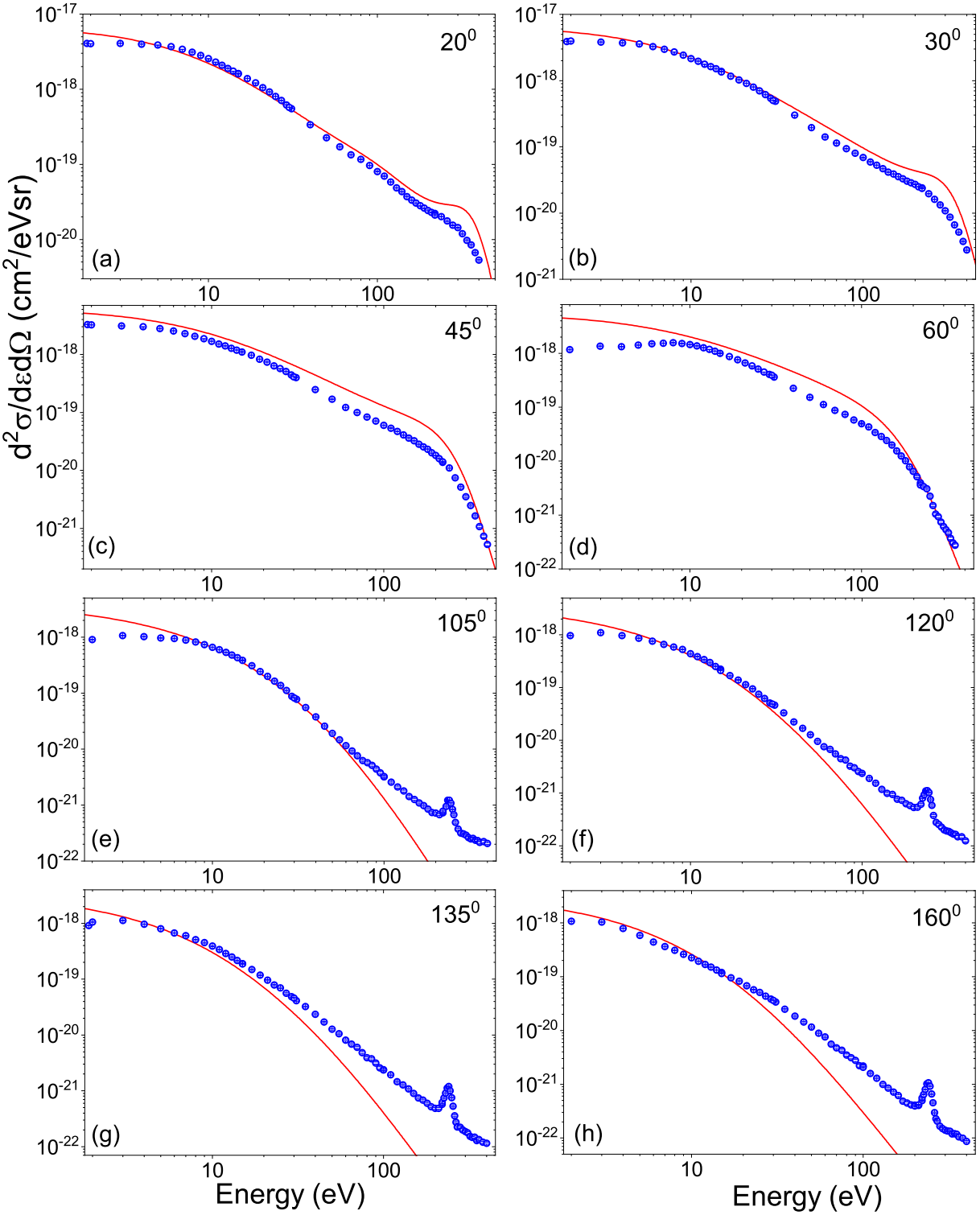

Figure 6.3: e-DDCS for the collision system 200 keV proton + CH_4; the prior form of the CDW-EIS calculations are shown by the red solid lines.

However, a mismatch is observed in case of the lowest electron energies (i.e., below 10 eV) for almost all the emission angles. Such a departure from the model in case of these low energy electrons could be due to the insufficient collection of electrons because of the presence of any stray electric or magnetic fields. The experimental uncertainties are large for these electrons

which adds up to other systematic errors.

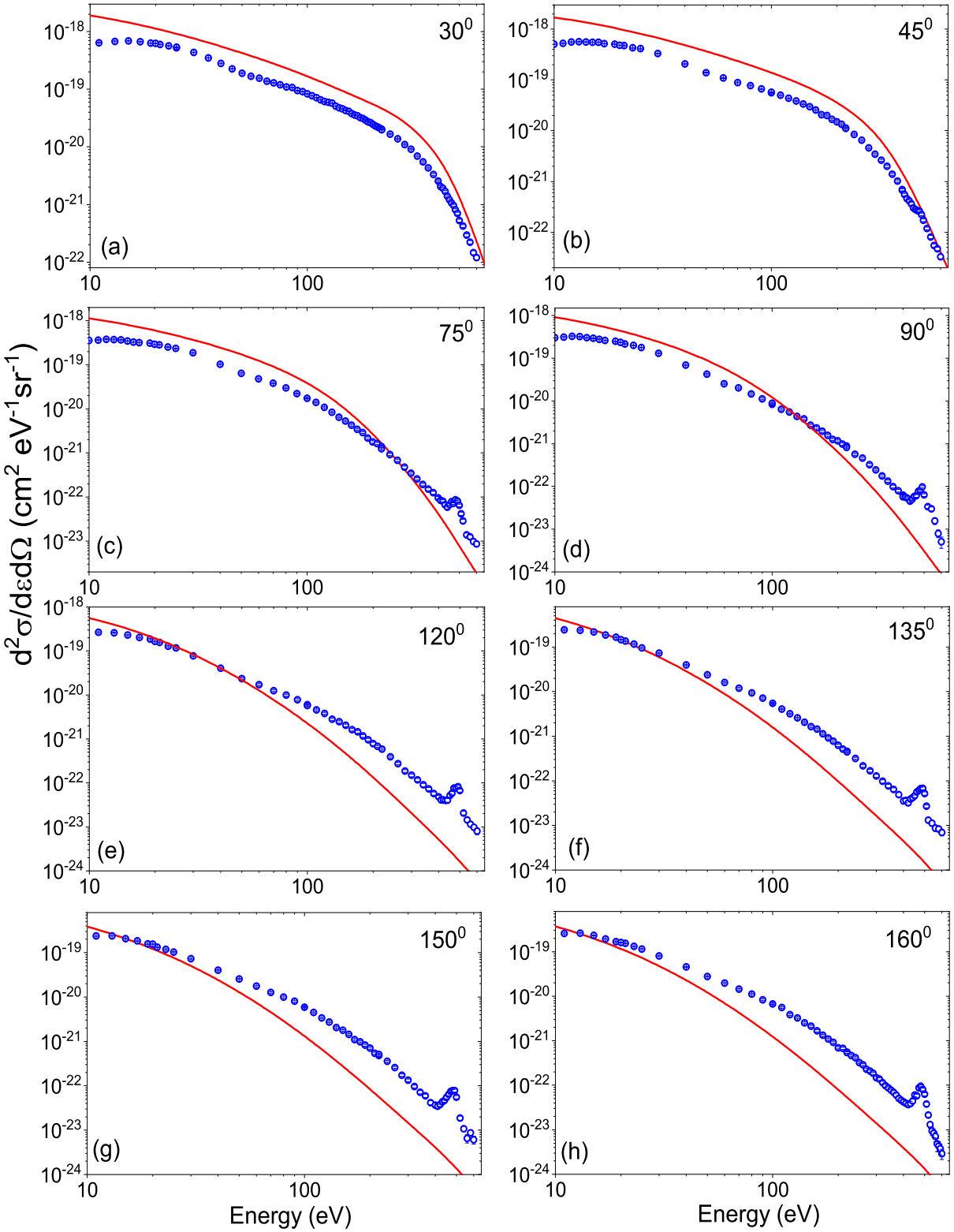

Figure 6.4: e-DDCS for the collision system 200 keV proton + O_2 along with the CDW-EIS calculations.

In Figure 6.3, the DDCS for 200 keV proton impact on CH_4 are shown for different forward

and backward emission angles. At about 240 eV, a sharp peak is seen in the backward angles. This peak corresponds to the K-LL Auger electron emission from carbon which occurs due to the presence of an inner shell vacancy. The prior form of the CDW-EIS calculations are shown by the red solid lines. In this model, the CH_4 molecule is represented by a Linear Combination of Atomic Orbitals (LCAO) within a Complete Neglect of Differential Overlap (CNDO) approximation [158, 170]. For the methane target, ε_i in Equation 6.4 is the molecular orbital ionization energy and n_i the principal quantum number of the corresponding atomic orbital in the LCAO combination. Overall an excellent agreement is observed between the CDW-EIS calculations and experimental data for 20^0 and 30^0. For 45^0 and 60^0, although qualitatively very good agreement is seen but quantitatively the model predicts slightly higher cross section than the data. In the backward angles, one observes a good agreement upto about 50 eV, beyond which theory underestimates the measured data. In the forward angles, a small hump like structure is observed which shifts towards the lower emission energy with increase in emission angles. This hump is due to the binary nature of collision or head-on collision between the projectile and the target electron. For 30^0 (Figure 6.3(b)) both the experimental measurements and the theoretical prediction show the hump around 250-300 eV. The position of the binary encounter (BE) peak is given by E=$4cos^2\theta m_e(\frac{E_p}{M_p})$, where M_p is the mass of the projectile having energy E_p, m_e is the mass of electron emitted with energy E at an emission angle θ. For 200 keV protons, the position of the peak should be at 300 eV and 200 eV for emission angles 30^0 and 45^0, respectively. If the target electron was initially at rest, then a prominent peak would have been expected. However, an electron bound to an atomic or molecular orbital has an initial momentum distribution which superimposes on the peak. For 200 keV protons, the projectile velocity is 2.83 a.u., which is close to the orbital velocity of the electrons (1 a.u.) in the outermost shell of CH_4. Thus the initial velocity distribution of the target electrons smears the binary peak over the entire emission energies resulting in the hump like structure.

Similarly, from Figure 6.4 one can see the electron emission DDCS spectra for O_2 when bombarded with 200 keV protons. As far as the CDW-EIS calculations are concerned, the O_2 molecule was approximated by two independent oxygen atoms and further described by RHF functions [102]. The residual target continuum state effective charge is given by Equation 6.4 where n_i is the principal quantum number of the atomic O orbital and ε_i its ionization energy. The solid curves represent the prior form of the calculations. It is seen that a large discrepancy exists between the measured data and the calculations for all the emission angles although any obvious reason for the same is not known. The peak at around 480 eV represents the K-LL Auger electron emission from oxygen. The peak is visible for all the backward angles whereas for forward angles they become invisible due to the large continuum cross sections.

The energy distribution of the electrons emitted from O_2 in collision with C^{6+} ions are shown in Figure 6.5. The low energy part of the spectrum is dominated by the soft collision mechanism where the electrons are emitted with large impact parameter. In case of highly

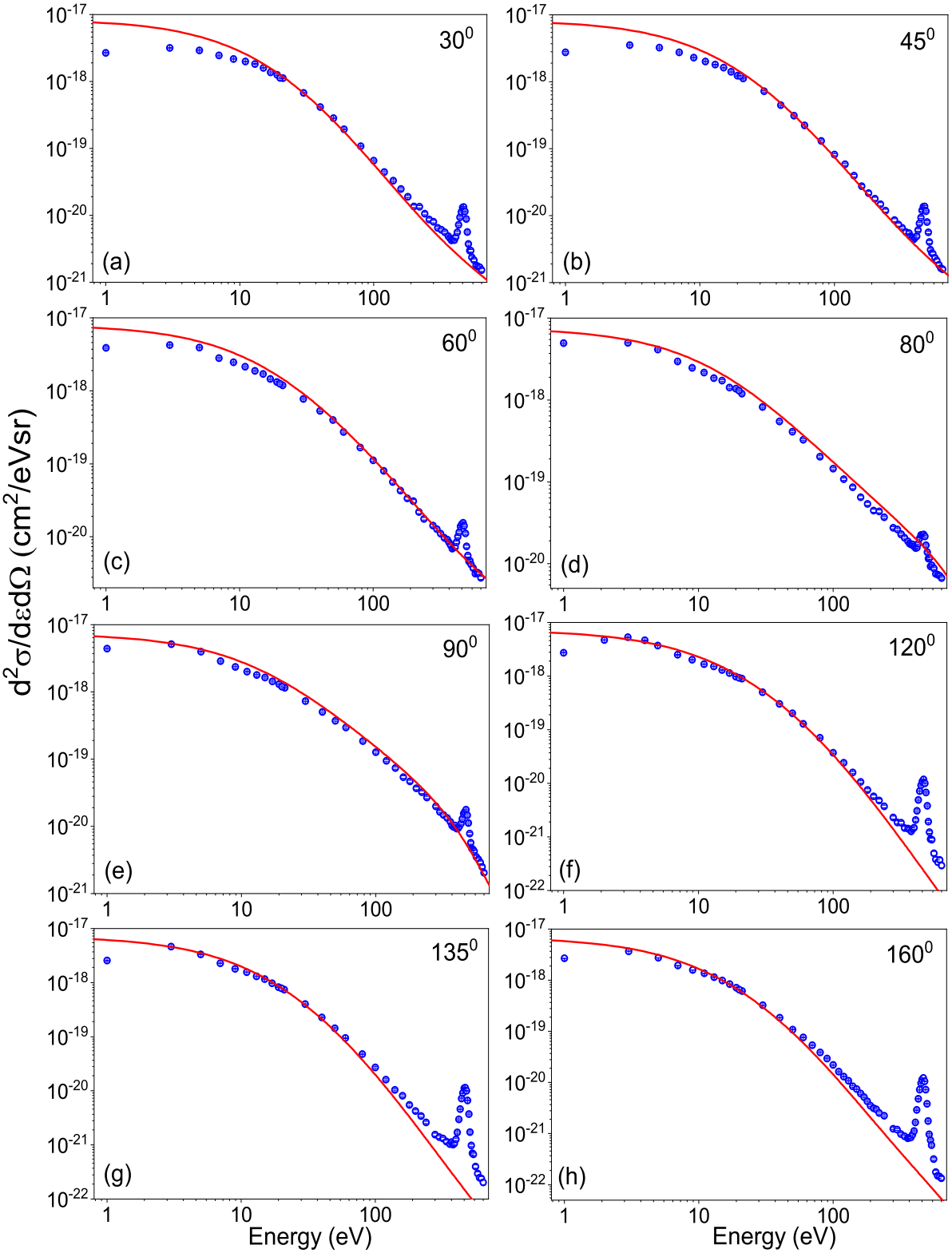

Figure 6.5: Absolute electron DDCS for the collision system 66 MeV C^{6+} + O_2, solid lines showing the CDW-EIS calculations.

charged ions like C^{6+}, two center effect plays an important role which gives rise to the intermediate part of the spectrum. Moving further ahead in the spectrum, the K-LL Auger peak at

$\sim$ 480 eV for oxygen are seen. For the present projectile, the velocity v_p is much larger ($\sim$ 15 a.u.) compared to the orbital velocity of the target electrons, and hence the BE peak will be present at a much higher emission energy in case of the extreme forward angles. The CDW-EIS model provides excellent agreement with the experimental data points for all the angles and over the entire energy range under consideration. Some deviations are observed only for the highest energy electrons at the extreme backward angles.

6.4 Post collision interactions

6.4.1 Angular distribution of DDCS

Figure 6.6 shows the angular distribution of the electrons ejected from the He target when collided with 150 keV protons for different electron emission energies. Figure 6.7, Figure 6.8 and Figure 6.9 display the DDCS as function of emission angles for 200 keV proton impact on He, CH_4 and O_2 respectively. From the above mentioned figures it is seen that a large angular asymmetry exist between the extreme forward and extreme backward angles even in case of low emission energies like 10 eV, 15 eV etc. The asymmetry increases even further with the increase in electron emission energy. This large angular asymmetry between the forward and backward angles may be explained by the two centre collision mechanism. The ionized electron experiences a strong interaction with the projectile, or in other words, the projectile drags away the electron along with it. This feature generates the large cross section in the forward angles. In case of the atomic target He, for either beam energies (Figure 6.6 and Figure 6.7), an excellent agreement is observed between the measured data and the theoretical model for low emission energies upto about 25 eV. With the increase in emission energies, although the model shows qualitative agreement with the measured quantities, but quantitatively it is seen that theory slightly overestimates the data for forward angles and underestimates the data points in the backward angles. For higher emission energies, the discrepancy increases even further for the backward angles. In Figure 6.8 and Figure 6.9, similar behaviour have been observed between the experimental data and CDW-EIS calculations for both the targets, CH_4 and O_2 in collisions with 200 keV H^+ ions. In all the cases, CDW-EIS model agrees qualitatively with data, but quantitatively shows wide deviation mainly at the backward angles for higher emission energies. In these figures, the total absolute error bars have been shown for some of the data points. From the angular distribution plots, it is observed that the CDW-EIS model agrees with the data particularly for forward angles, thus accounting well on the post collision interactions.

In Figure 6.10, the DDCS of electrons as a function of emission angles for 66 MeV C^{6+} ion impact on O_2 have been displayed. The angular distribution plots shown in the eight panels for fixed electron energies show completely different trend to that observed in Figure 6.9. In case of 11 eV (Figure 6.10(a)), an almost flat distribution is observed over the entire angular region

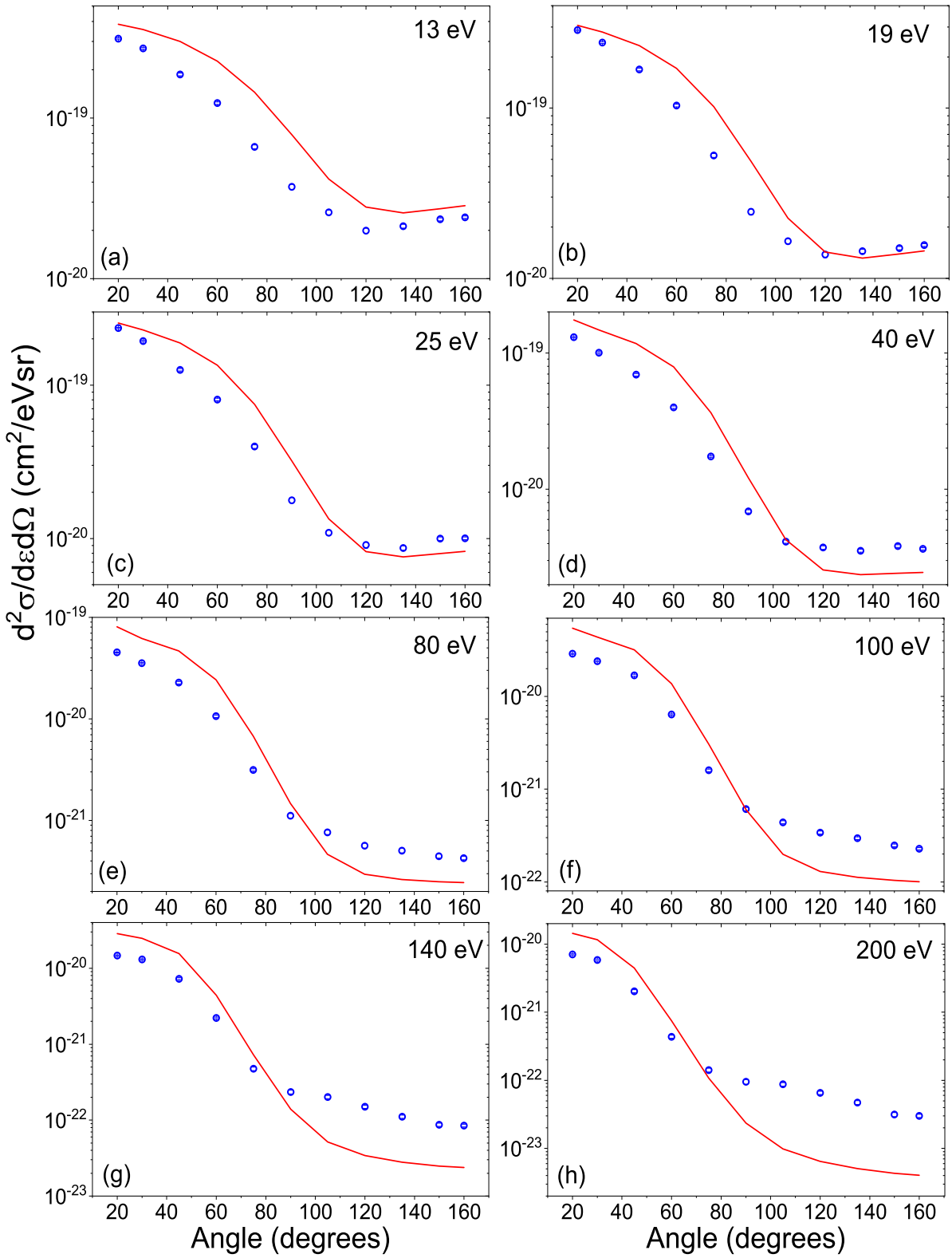

Figure 6.6: Absolute electron DDCS as a function of emission angles for the collision system 150 keV H^+ ion impact on He along with the CDW-EIS calculations.

between 20^0 and 160^0. This is due to the dominance of soft collision mechanism, indicating isotropic ionization over all angles. With increase in emission energies, the forward angles

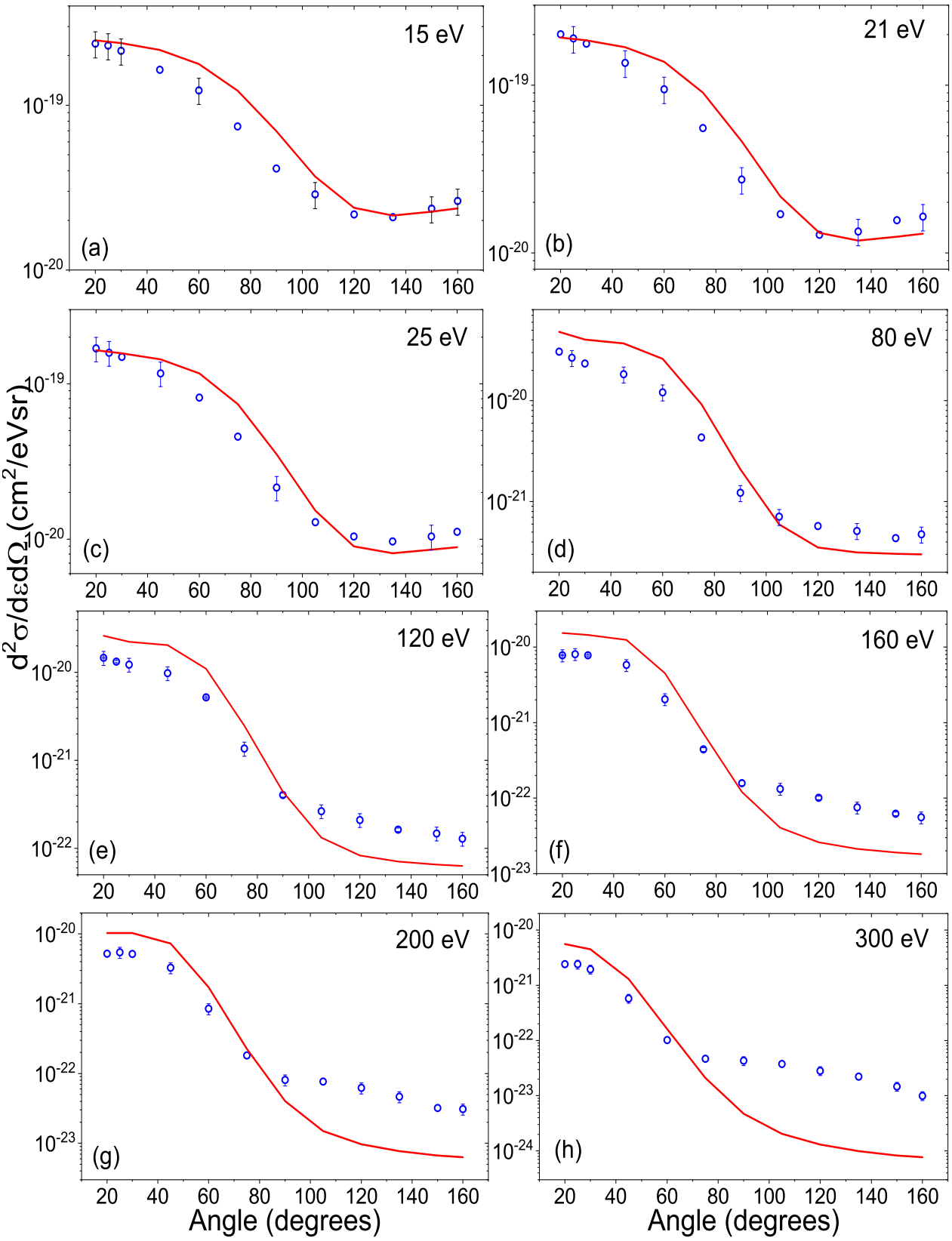

Figure 6.7: Angular distribution of electron DDCS for 200 keV proton impact on He at fixed electron emission energies as indicated in panels along with the theoretical calculations.

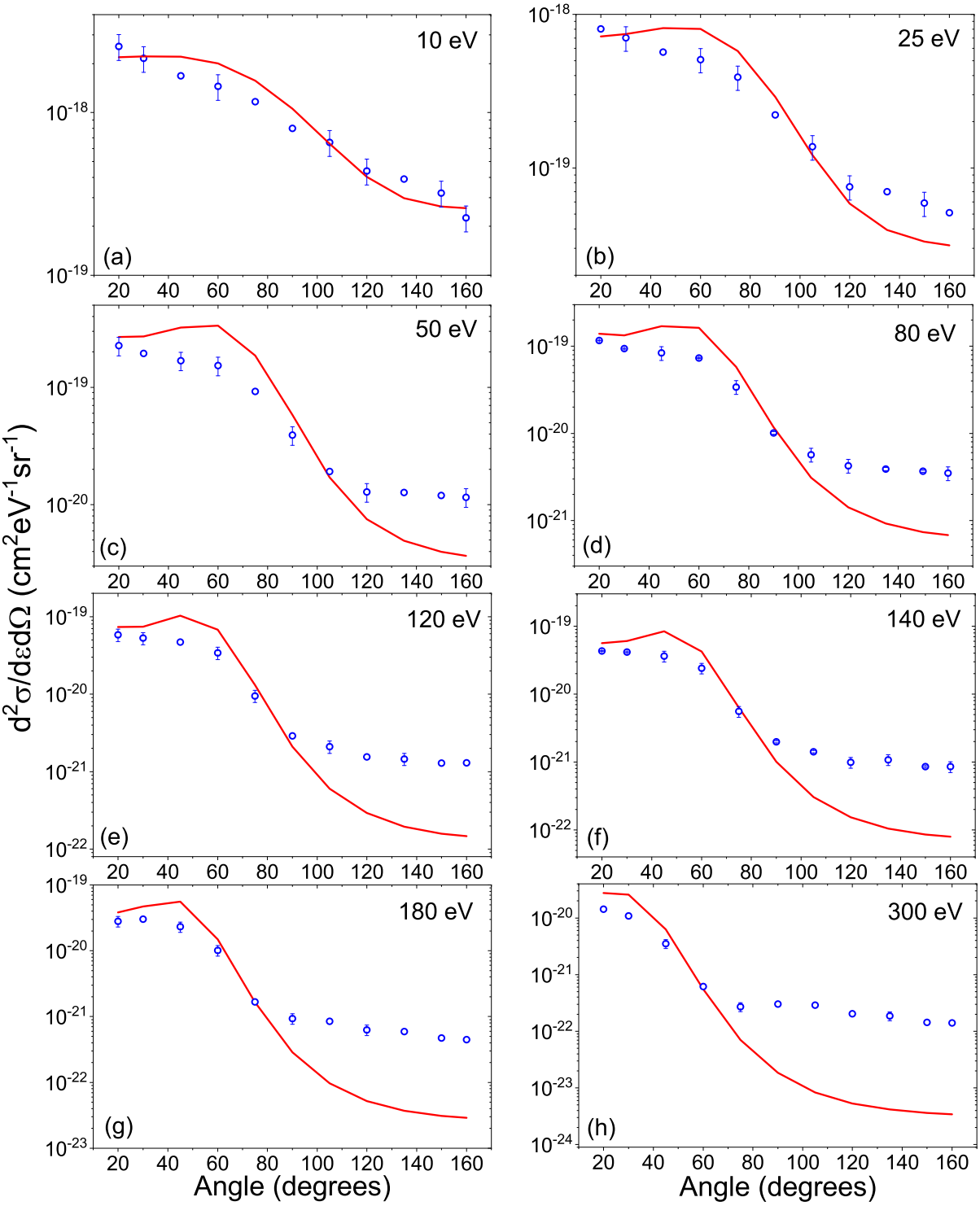

Figure 6.8: Same as Figure 6.7, except for the collision system : 200 keV proton impact on CH_4.

have higher cross sections compared to the backward angles which is due to the two centre effect. For 80 eV (Figure 6.10(d)), the DDCS for extreme forward angles are 2.7 times higher than the extreme backward angles. This factor increases further with higher emission energies and in case of 340 eV, it is about 6 times higher than backward angles, indicating a drastic

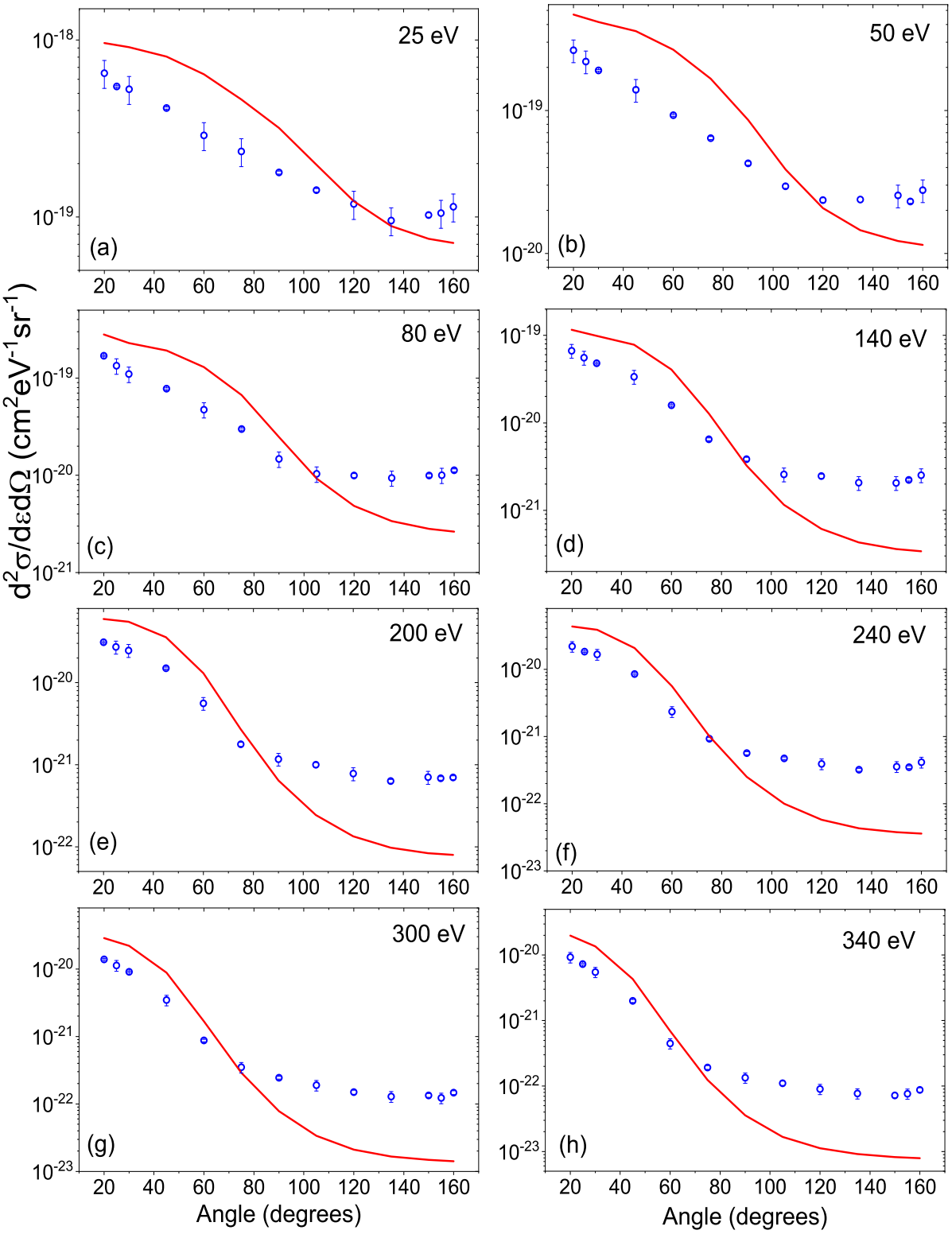

Figure 6.9: Angular distribution of the DDCS for the collision system : 200 keV proton impact on O_2, red line showing the CDW-EIS calculations.

fall of cross sections in case of backward angles. Although the cross sections are higher in the forward angles compared to the backward ones, but they are not as large as that seen in

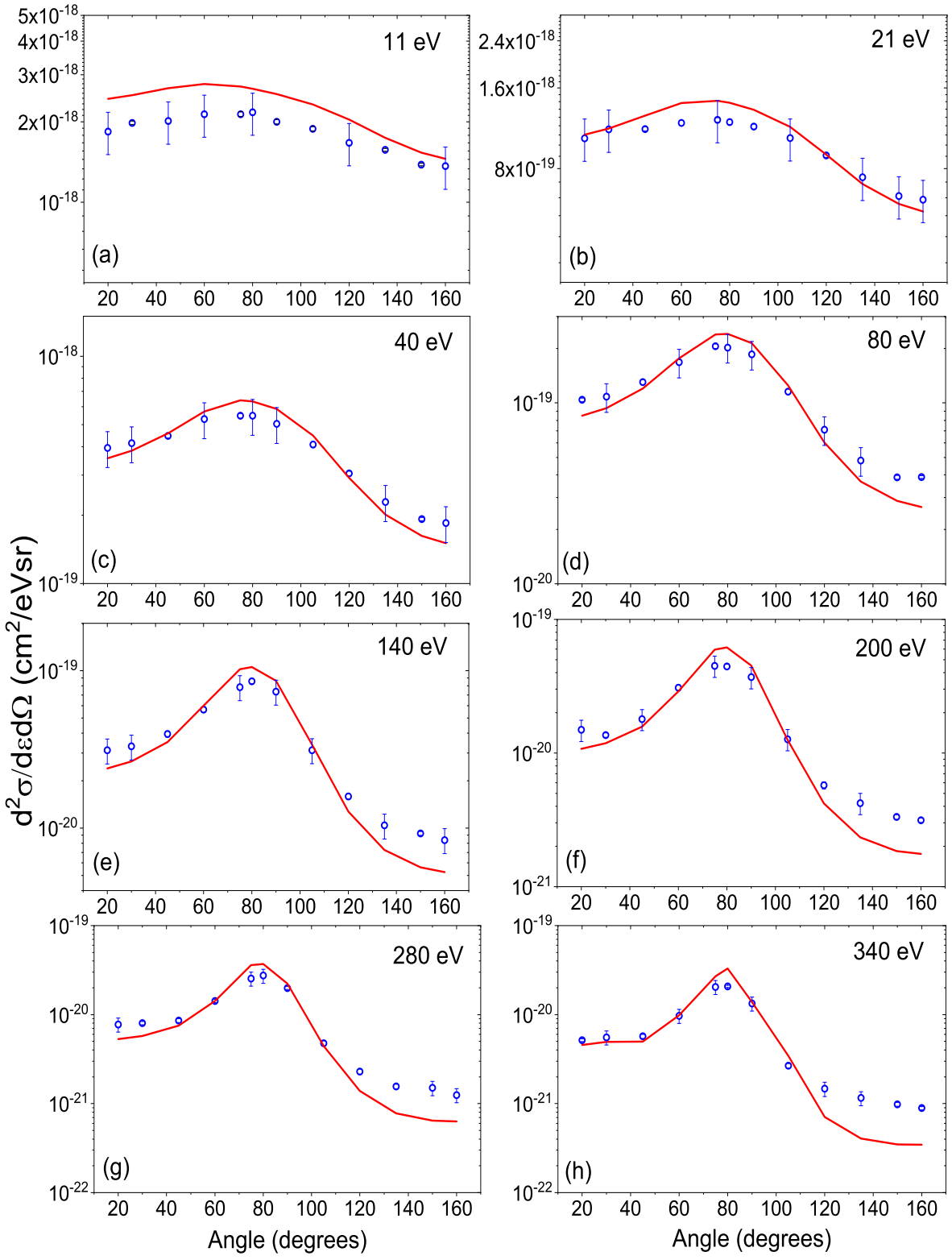

Figure 6.10: Same as Figure 6.9, except for collision system : 66 MeV C^{6+} + O_2

Figure 6.9. In Figure 6.9(a), for 25 eV emission energy, the DDCS at 20^0 is 5.6 times higher than at 160^0, whereas in Figure 6.10(b) this difference is 1.7 times for 21 eV electron energy. Thus, although for high velocity highly charged ions two center effect causes higher DDCS in

forward angles but, due to the high velocity the projectile moves away quite fast. On the other hand, for intermediate velocity protons the influence of the projectile on the electrons in the forward direction is extremely strong. For higher electron energies, a peak is observed around 80^0 (Figure 6.10) which gets sharper with increase in electron emission energy. This peak is due to the binary collision mechanism. The CDW-EIS model shows an excellent agreement with the data for the 66 MeV bare C ions, reproducing the collision mechanisms very nicely. Deviations are observed only for the highest energy electrons in the backward angles, where it underestimates the data.

6.4.2 Forward backward angular asymmetry

Following the prescription of Fainstein *et al*[109], the forward-backward angular asymmetry parameter ($\alpha(k)$) is defined as:

$$\alpha(k,\theta) = \frac{\sigma(k,\theta) - \sigma(k,\pi-\theta)}{\sigma(k,\theta) + \sigma(k,\pi-\theta)} \tag{6.5}$$

here the electron energy $\epsilon_k = \frac{k^2}{2}$ in a.u., θ is a low forward angle and k denotes the ejected electron velocity. As the angular distribution vary slowly near 0 and π, so the measured DDCS at 20^0 was used to calculate the approximate value of the asymmetry parameter i.e. $\alpha(k)$ for all the five collision systems under investigation (shown in Figure 6.11). In Figure 6.11(a), Figure 6.11(b) and Figure 6.11(c) it is seen that a large asymmetry exist for He and CH_4 which increases monotonically from 0.7 to $\sim$ 1.0, showing a tendency to saturate beyond $k = 2.75$ a.u. The CDW-EIS model predicts similar behaviour. The model shows an excellent agreement for He for both the projectile energies (Figure 6.11(a), Figure 6.11(b)). However, experimentally CH_4 shows a slightly different shape compared to the theoretical predictions as well as that observed for He. For 200 keV protons colliding on the O_2 target, the $\alpha(k)$ increases monotonically from 0.4 to ~ 1.0 and saturates beyond 2.75 a.u. (see Figure 6.11(d)). It is seen that although the shape of the angular distributions due to collisions at the lower energy i.e, keV (Figure 6.9) and higher energy i.e., MeV (Figure 6.10) are vastly different but the asymmetry parameter reveals almost similar distributions as a function of k (Figure 6.11(e)). Thus $\alpha(k)$ can be used as a tool to compare the data at widely different projectile energy range. It is obvious from Figure 6.11(e) that the $\alpha(k)$ values for 200 keV/u protons are much larger than that for the collisions with the MeV energy C^{6+} ions. This may be explained by the fact that two centre effect and post collisional interactions are much stronger for 200 keV protons compared to the MeV energy projectiles, although the perturbation strength i.e. (q_p/v_p) for both the projectiles are nearly same. Thus, asymmetry parameter cannot be characterised uniquely by the perturbation strength, rather it depends independently on the actual value of the charge state (q_p) and the velocity (v_p). It is further noticed from Figure 6.11(f) that for lower electron energies the asymmetry parameter is sensitive to the atomic or molecular structure of the target

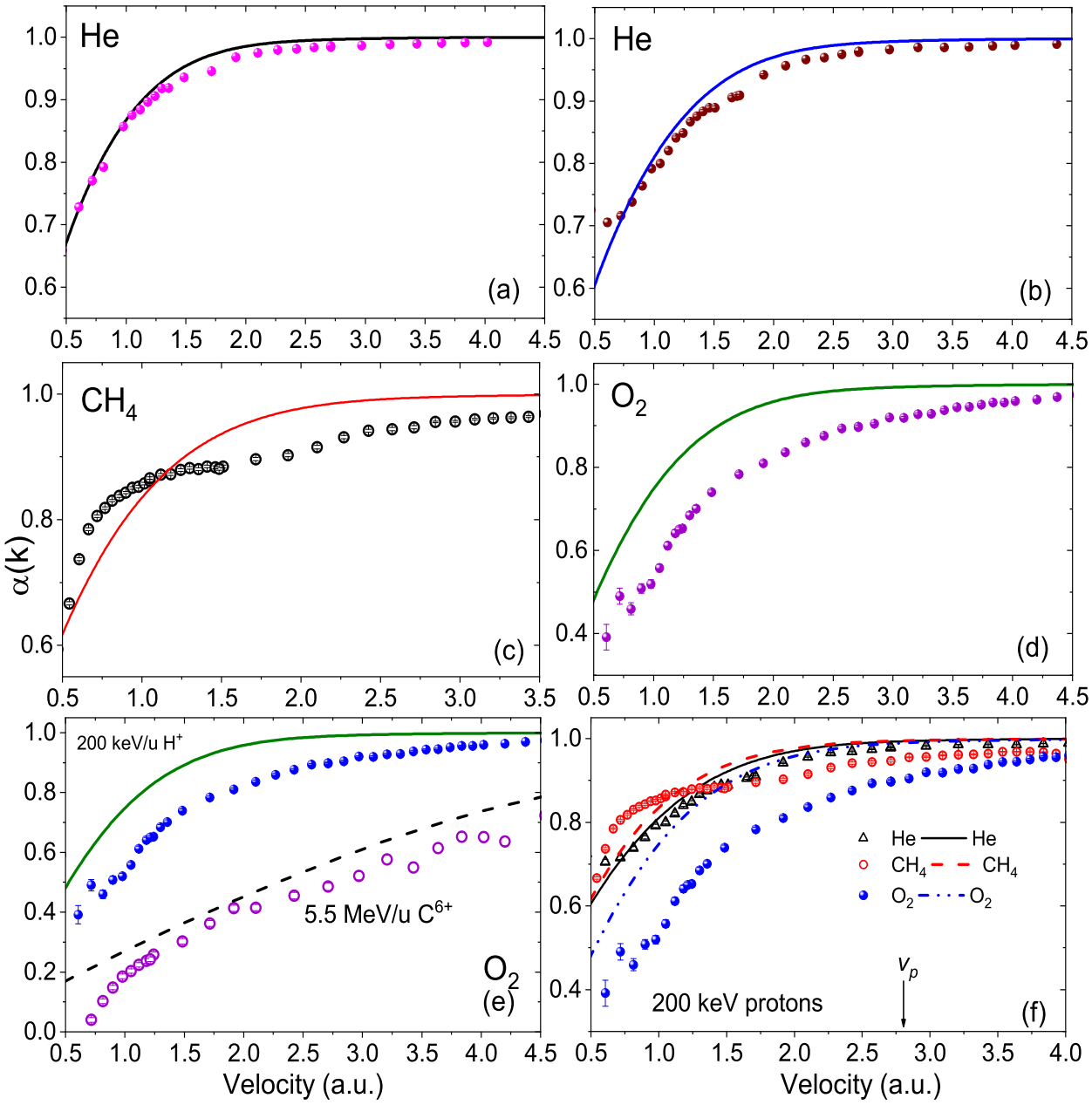

Figure 6.11: Asymmetry parameter ($\alpha(k)$) for different collision systems (a) 150 keV H^+ + He (b) 200 keV H^+ + He (c) 200 keV H^+ + CH_4 (d) 200 keV H^+ + O_2 (e) 200 keV H^+ + O_2 and 66 MeV C^{6+} + O_2 (f) three different targets bombarded by the same projectile.

and is having the least value for O_2, followed by the He and CH_4 targets, when bombarded by the same projectile. In case of these low energy electrons, the impact parameters are expected to be large and hence the projectile interacts with the whole atom or molecule. Here the momentum transfer is small and thereby the ejected electrons are sensitive to the structure of the atom or the molecule. As the velocity of the electron increases along the X axis, the $\alpha(k)$ tend to merge together. This is because for these electron velocities, the impact parameter is quite small and hence the projectile interacts mostly with individual atoms in the molecule. Another feature that is observed for all the three targets (He, CH_4 and O_2) is the saturation effect. This

effect is showing up when the electron velocity is close to or above the velocity of the projectile (v_p). In case of 5.5 MeV/u C^{6+} ions, the projectile velocity being much higher than the highest value of k measured in these experiments, the $\alpha(k)$ values keep on increasing with the increase in the electron velocity and no saturation behaviour is observed. Thus the angular asymmetry is another or complementary way to extract information about the collision dynamics and its dependence on molecular species.

6.5 Single differential cross section

The single differential cross section (SDCS) can be obtained from the measured DDCS by integrating over one of the variables, either the measured emission energies or the emission angles.

$$\frac{d\sigma}{d\Omega_e} = \int \frac{d^2\sigma}{d\Omega_e d\epsilon_e} d\epsilon_e. \tag{6.6}$$

$$\frac{d\sigma}{d\epsilon_e} = \int \frac{d^2\sigma}{d\epsilon_e d\Omega_e} d\Omega_e. \tag{6.7}$$

Figure 6.12 shows the SDCS as a function of emission angles for all the five collision systems studied in this chapter. Figure 6.12(a) shows the SDCS for 150 keV proton impact on the He target and Figure 6.12(b) displays those for 200 keV proton impact on the three targets He, CH_4 and O_2. Figure 6.12(c) displays the SDCS for 66 MeV bare C ions impacting on O_2. The solid and dashed lines in all the three panels in Figure 6.12 show the theoretical predictions. The SDCS obtained experimentally and theoretically for CH_4 have been multiplied by a factor of 4 (shown in Figure 6.12(b)). For all the three targets, the SDCS have been obtained by integrating the data from 5 eV to 400 eV. In case of He it is observed that the CDW-EIS prediction matches well with the experimentally obtained SDCS for both the beam energies, although slightly overestimates the data below 120^0. In case of CH_4, the theory overall shows a qualitative agreement with an excellent matching between 100^0 and 120^0(Figure 6.12(b)). Contrary to the cases observed for He and CH_4, in case of 200 keV proton impact on O_2 (see Figure 6.12(b)), a wide deviation is observed between experimental and theoretical SDCS almost over the entire angular region. However, for high energy highly charged ions impacting on O_2 (see Figure 6.12(c)), the angular variation of SDCS from the experimental measurements is reproduced very well by the theoretical model with an excellent agreement for the backward angles.

Integrating the SDCS over the emission angles, the total ionization cross section (TCS) of the collision system is obtained. The TCS values provided in Table 6.1 have been deduced by integrating over the electron energies from 5 to 400 eV and over the emission angles between 20^0 and 160^0. The theoretical to experimental TCS ratios provide best agreement for MeV

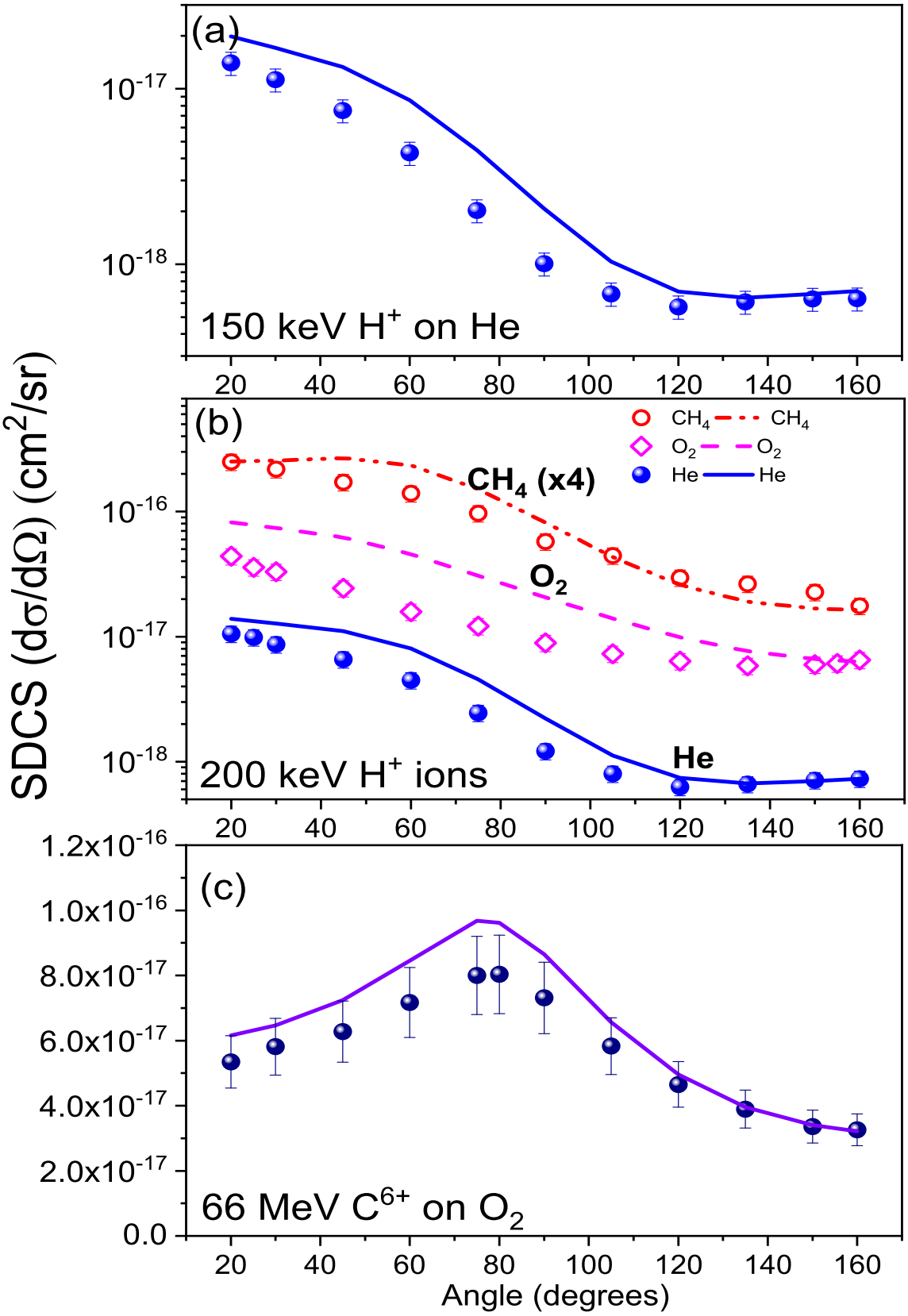

Figure 6.12: SDCS as a function of emission angle (a) 150 keV H^+ + He (b) 200 keV proton impact on He, CH_4 and O_2 (c) 66 MeV C^{6+} on O_2. The solid and dashed lines correspond to the CDW-EIS calculations.

Table 6.1: Total ionization cross section (TCS) in units of Mb for the five collision systems

Target	Projectile	q_p/v_p	TCS Expt($\pm 18\%$)	TCS CDW-EIS	Ratio
He	150 keV/u H^+ ions	0.41	33.3	57.6	1.7
He	200 keV/u H^+ ions	0.35	31.5	50.7	1.6
CH_4	200 keV/u H^+ ions	0.35	252	346	1.4
O_2	200 keV/u H^+ ions	0.35	148	337	2.3
O_2	5.5 MeV/u C^{6+} ions	0.40	708	809	1.14

energy highly charged ion projectile. For keV energy protons, the deviations vary by a factor of 1.4 to 2.3 with maximum difference occurring in case of 200 keV proton impact on O_2. From this study it may be inferred that although the perturbation strengths ((q_p/v_p)) were nearly the same for all these five collision systems, but the difference between the data and the model is not the same, showing larger deviation for keV energy projectile.

6.6 Conclusions

In conclusion, we have studied the variation in the collision dynamics for atoms and molecules when ionized by keV energy protons and MeV energy bare C ions. The absolute DDCS of the electrons emitted from He were measured for projectiles 150 keV and 200 keV protons. In addition, e-DDCS measurements were also carried out for two molecular targets CH_4 and O_2 when ionized by 200 keV/u protons along with that for O_2 in collisions with 5.5 MeV/u bare C ions. The energy of the projectiles and their charge state were chosen such that the perturbation strength were nearly the same for all of them. In case of 66 MeV bare C ions, the CDW-EIS calculations for oxygen showed an excellent agreement with the measured data for all the angles. For He, the model provided reasonably good agreement for both 150 keV and 200 keV protons. Similarly, for 200 keV proton impact on CH_4, the calculations showed good agreement with the experimental DDCS. However, for single ionization of O_2 by keV energy protons, the model overestimates the data in case of all the emission angles. The angular distribution revealed a distinctly different character for the two different projectiles. In case of keV energy collisions, the forward backward asymmetry parameter has much higher value compared to that for MeV energy bare C ions, although the perturbation strength were nearly similar. This indicates that the perturbation strength (q_p/v_p) alone cannot characterize completely the asymmetry and two center effect. For 150 and 200 keV protons, $\alpha(k)$ showed a saturation effect for all the three targets when the electron velocity is greater than the velocity of the projectile. The single differential distributions and total cross sections are also derived. The CDW-EIS provides best agreement for the collisions with 5.5 MeV/u bare C ions whereas deviations (by a factor of

1.4 to 2.3) exist for the keV energy protons with maximum difference occurring in case of O_2, inspite of having nearly same perturbation strength for all the collisions. Further systematic investigations are required to check the efficacy of perturbation strength in characterizing the collision dynamics.